doi:10.1016/j.jmb.2007.11.097 J. Mol. Biol. (2008) 376, 570–581

JMB

Available online at www.sciencedirect.com

ScienceDirect

ELSEVIER

Structural Analysis of the PP2C Phosphatase tPphA from *Thermosynechococcus elongatus*: A Flexible Flap Subdomain Controls Access to the Catalytic Site

Christine Schlicker[1,2]*, Oleksandra Fokina[3], Nicole Kloft[4], Tim Grüne[1], Stefan Becker[5], George M. Sheldrick[1] and Karl Forchhammer[3,4]

[1]*Department of Structural Chemistry, Georg-August-University, Tammannstrasse 4, 37077 Göttingen, Germany*

[2]*Department of Physiological Chemistry, Ruhr-University Bochum, Universitätsstrasse 150, 44801 Bochum, Germany*

[3]*Department of Microbiology/ Organismic Interactions, University of Tübingen, Auf der Morgenstelle 28, 72076 Tübingen, Germany*

[4]*Institute of Microbiology and Molecular Biology, Justus-Liebig-University Giessen, 35392 Giessen, Germany*

[5]*Department of NMR-based Structural Biology, Max-Planck-Institute for Biophysical Chemistry, Am Fassberg 11, 37077 Göttingen, Germany*

Received 4 September 2007; received in revised form 22 November 2007; accepted 29 November 2007
Available online
5 December 2007

Edited by G. Schulz

The homologue of the phosphoprotein PII phosphatase PphA from *Thermosynechococcus elongatus*, termed tPphA, was identified and its structure was resolved in two different space groups, $C222_1$ and $P4_12_12$, at a resolution of 1.28 and 3.05 Å, respectively. tPphA belongs to a large and widely distributed subfamily of Mg^{2+}/Mn^{2+}-dependent phosphatases of the PPM superfamily characterized by the lack of catalytic and regulatory domains. The core structure of tPphA shows a high degree of similarity to the two PPM structures identified so far. In contrast to human PP2C, but similar to *Mycobacterium tuberculosis* phosphatase PstP, the catalytic centre exhibits a third metal ion in addition to the dinuclear metal centre universally conserved in all PPM members. The fact that the third metal is only liganded by amino acids, which are universally conserved in all PPM members, implies that the third metal could be general for all members of this family. As a specific feature of tPphA, a flexible subdomain, previously recognized as a flap domain, could be revealed. Comparison of different structural isomers of tPphA as well as site-specific mutagenesis implied that the flap domain is involved in substrate binding and catalytic activity. The structural arrangement of the flap domain was accompanied by a large side-chain movement of an Arg residue (Arg169) at the basis of the flap. Mutation of this residue strongly impaired protein stability as well as catalytic activity, emphasizing the importance of this amino acid for the regional polysterism of the flap subdomain and confirming the assumption that flap domain flexibility is involved in catalysis.

Keywords: PII signalling; PphA; cyanobacteria; PPM phosphatase

**Corresponding author.* Department of Physiological Chemistry, Ruhr-University Bochum, Universitätsstrasse 150, 44801 Bochum, Germany. E-mail address: c_schlicker@yahoo.de.

Abbreviations used: tPphA, homologue of the phosphoprotein PII phosphatase PphA from *Thermosynechococcus elongatus*; PP2C, phosphatase 2C; PstP, PPM phosphatase from *Mycobacterium tuberculosis*; MspP, PPM phosphatase from *Mycobacterium smegmatis*; 2-OG, 2-oxoglutarate; STP, PPM member from *Streptococcus agalactiae*; *p*-NPP, *p*-nitrophenyl phosphate; MAD, multiple wavelength dispersion.

Introduction

Signal transduction based on the reversible phosphorylation of proteins on seryl and threonyl residues is one of the most universal mechanisms employed by living cells to control cellular processes and adapt to changes in the environment. In addition to protein Ser/Thr kinase activity, these signal transduction pathways require the activity of protein Ser/Thr phosphatases. These comprise two large families, the PPP family and the Mn^{2+}/Mg^{2+}-dependent PPM family. Members of these families are found in all domains of life, including eukarya, archaea and bacteria.[1,2] In the bacterial kingdom, genome sequencing revealed an unexpectedly frequent occurrence of PPM homologues in those phylogenetic groups whose members may exhibit complex life cycles, such as the actinobacteria and cyanobacteria.[2–4] The eukaryotic PPM member protein phosphatase 2C (PP2C) is involved in the reversal of protein kinase cascades, which become activated as a result of stress. In spite of the increasing number of genes that encode bacterial PPM homologues, knowledge of their physiological roles and functional interactions is still limited. Based on the conservation of the 11 sequence motifs characteristic of PPM members, the PPM family was subdivided into two subfamilies: The members of subfamily I, including eukaryotic PP2C, have conserved all 11 motifs, whereas the members of subfamily II, exclusively found in bacteria, lack motifs 5a and 5b.[2,4] Another classification, according to domain architecture, groups mammalian PP2C together with several prokaryotic PPMs in a class in which the catalytic domain is fused either to C- or N-terminal regulatory or substrate-binding domains (termed class 1). In contrast, class 2 consists of various bacterial PPM homologues that are small enzymes consisting of only the catalytic core.[5]

The genomes of cyanobacteria are particularly rich in PPM homologues, indicating that protein Ser/Thr phosphorylation plays an important role in modulation of cellular functions in this bacterial phylum.[3] The unicellular, nondiazotrophic cyanobacterium *Synechocystis* displays as much as eight genes encoding PPM homologues.[2] The filamentous, multicellular cyanobacterium *Nostoc* PCC 7120 may contain as much as 12 PPM homologues.[6] One of the most thoroughly studied regulatory pathways involving the function of a PPM homologue in cyanobacteria is the P_{II} signal transduction system.[7,8] P_{II}-like proteins represent one of the most widely distributed classes of signalling proteins in nature; they control nitrogen-assimilatory processes in bacteria, archaea and autotrophic eukaryotes.[9–11] In a variety of cyanobacteria, including the unicellular strains *Synechocystis* PCC 6803 and *Synechococcus elongatus* PCC 7942 and PCC 6301, the P_{II} signal transduction protein is phosphorylated on a seryl residue (Ser49) located at the apex of a large, solvent-exposed loop, termed T loop. P_{II} homologues in other bacteria are not phosphorylated but may be either uridylylated or adenylylated at a neighbouring tyrosyl residue (Tyr51). The phosphorylation state of the P_{II} protein from unicellular cyanobacteria was shown to respond to the cellular carbon and nitrogen supply as well as to illumination conditions.[7,8,12] The P_{II} protein is a sensor of the cellular levels of the metabolites 2-oxoglutarate (2-OG) and ATP, which are bound by P_{II} in a synergistic manner. In the presence of ATP, binding of 2-OG, the indicator of cellular carbon/nitrogen balance in cyanobacteria, results in P_{II} phosphorylation. As long as phosphorylated P_{II} (P_{II}-P) is complexed to its effector molecules, it is resistant towards dephosphorylation. However, when 2-OG dissociates from P_{II}-P following a drop in its level (e.g., in response to increased combined nitrogen supply), P_{II}-P is rapidly dephosphorylated.[7,8,13] The corresponding enzyme, termed PphA, was identified in *Synechocystis* PCC 6803 and was shown to be a member of the PPM family.[14]

PphA has conserved the 11 motifs of the PP2C family and is a member of the large group of bacterial PPMs consisting of just the catalytic core. Members of this group of enzymes are found in numerous bacteria, including pathogenic and non-pathogenic strains.[2–4] However, it is still unknown how these enzymes, despite the lack of obvious substrate recognition and regulatory domains, specifically recognize their substrates and tune their activity. *In vivo* studies showed that in *Synechocystis* PCC 6803 only PphA is able to dephosphorylate P_{II}-P rapidly, although seven other PPM members are present.[15] Structure–function analysis with regard to substrate recognition and activity regulation of this group of enzymes was hampered so far by the lack of a crystal structure. Recently, the crystal structure of the catalytic domain of a membrane-anchored bacterial PPM member from *Mycobacterium tuberculosis* (PstP) was reported,[16] as well as the structures of a soluble PPM phosphatase from *Mycobacterium smegmatis* (MspP)[17,18] and *Streptococcus agalactiae* (STP).[19] These structures showed high overall degree of structural conservation as compared to the human PP2C homologue,[20] with the most striking difference being the presence of a third metal ion in the catalytic centre, compared to two Mn^{2+} ions in mammalian PP2C. To gain more insight into the function and regulation of the small soluble protein phosphatases, we aimed to unravel the structure of the cyanobacterial PphA homologue. In this article, the structure of the *Thermosynecococcus elongatus* homologue of PphA is presented and a mutational analysis gives first insights into regions outside the catalytic centre involved in substrate turnover and recognition.

Results and Discussion

Thermosynechococcus elongatus Tll2243 is the functional homologue of protein phosphatase PphA from *Synechocystis* PCC 6803

Initial attempts to crystallize the *Synechocystis* PCC 6803 PphA protein were unsuccessful. Only thin

plates that diffracted only to low resolution could be obtained. Therefore, we attempted the crystallization of the PphA homologue from the thermophilic cyanobacterium *T. elongatus*. BLAST searches and ClustalW[21] multiple sequence alignment revealed tll2243 as the closest relative of PphA, with the two proteins exhibiting an amino acid sequence identity of 51% (Fig. 1a). In addition to the high similarity in the conserved PP2C motifs,[22] the high sequence similarity in a region of poor conservation among PP2C members is of particular significance. In the crystal structure of the *M. tuberculosis* PPM member PstP,[16] this part of the protein was shown to form a flap subdomain located in the vicinity of the catalytic site. The structure of this subdomain is not conserved compared to that of human PP2C.[20] Figure 1b shows the primary sequences corresponding to the region of the PstP flap subdomain of PphA and Tll2243 compared to five cyanobacterial PPM members. Of those, three PPM members are from *Synechocystis* PCC 6803: the two phylogenetically closest neighbours of PphA (the products of sll1033 and sll0602), as well as the distantly related IcfG (slr1860 product). The tll1664 product is a closely related PPM member in *T. elongatus*, and PrpS (all4516 product) is the functional homologue of PphA in *Anabaena* sp. PCC 7120.[23] As is apparent from this comparison, this region is highly conserved between PphA, PrpS and Tlr2243, whereas the other phosphatases show only low similarity. The similarity of Tll2243 with the P_{II}-specific phoshatases is in accord with the assumption that Tlr2243 is the functional homologue of PphA in *T. elongatus*.

To verify that the tll2243 product has biochemical properties similar to those of PphA, the *tll2243* gene was overexpressed in *Escherichia coli* and the product was purified to homogeneity. Enzymatic assays were carried out to compare the properties of Tll2243 with those of PphA. First, the reactivity towards the artificial broad-range substrate *p*-nitrophenyl phosphate (*p*-NPP) was studied. Similar to the activity of PphA,[13] Tll2243 requires Mn^{2+} ions with an optimum of 2 mM for reactivity against *p*-NPP and a pH above 8 (data not shown). The reactivity towards phosphorylated P_{II} protein and the modulation of this reaction by the P_{II} effector molecules ATP and 2-OG were tested subsequently. As shown in Fig. 2a, Tll2243 is able to dephosphorylate P_{II}-P in the presence of either Mn^{2+} (not shown) or Mg^{2+} as divalent ions, similar to the data reported

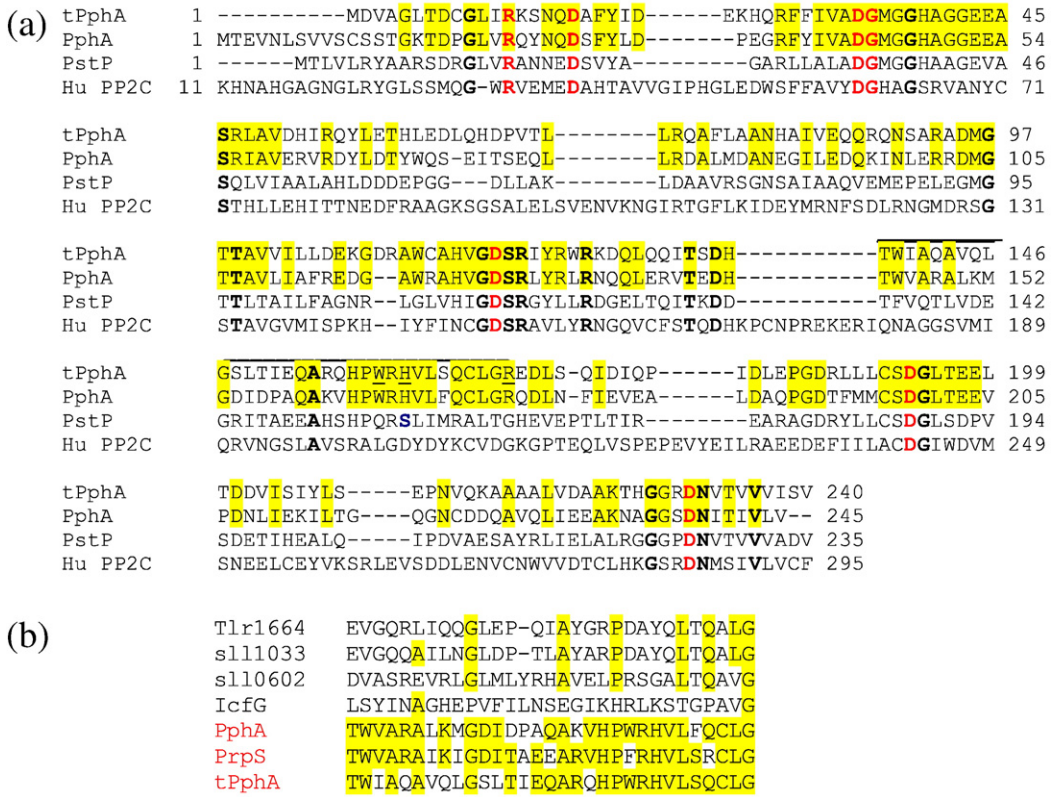

Fig. 1. Sequence comparisons between the sll2243 product (tPphA) and various PP2C homologues. (a) Comparison between tPphA from *T. elongatus*, PphA (the P_{II}-P phosphatase from *Synechocystis* sp. PCC 6803), and the two PP2C members of known 3D structure, PstP (from *M. tuberculosis*) as well as human PP2C. Amino acids conserved in all proteins are indicated by bold letters. Among those, the residues that form part of the metal-binding pocket are labelled in red. Identities between Sll2243 and PphA are highlighted by a yellow background. (b) Comparison of the amino acid sequence in the flap subdomain of various cyanobacterial PP2C members: IcfG, Sll1033, Sll0602 and PphA from *Synechocystis* PCC 6803, tPphA and Tlr1664 from *T. elongatus* and PrpS from *Anabaena* sp. PCC 7120. Identities within the PphA/tPphA/PrpS cluster are highlighted by yellow background.

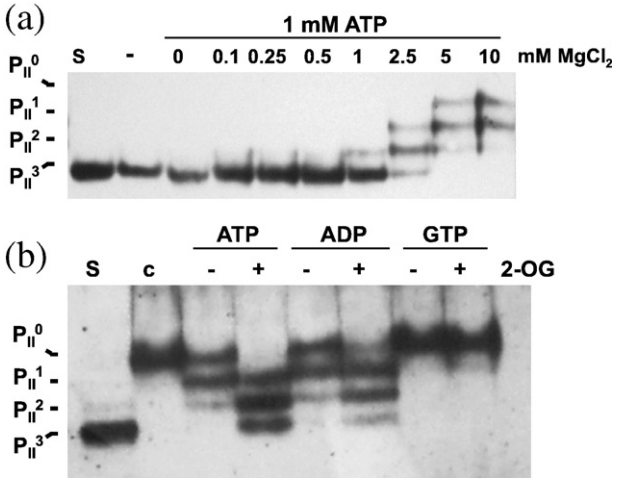

Fig. 2. Dephosphorylation of P_{II}-P by the sll2243 product (tPphA). (a) Dependence of tPphA-catalyzed P_{II}-P dephosphorylation on the Mg^{2+} concentration. Reactions were carried out as described in Materials and Methods, except that $MgCl_2$ was present in the dephosphorylation reaction at concentrations as indicated. (b) Dependence of tPphA-catalyzed P_{II}-P dephosphorylation on P_{II} effector molecules. The concentration of ATP, ADP or GTP was 1 mM. Where indicated, 2-OG was added to a final concentration of 0.5 mM.

previously for PphA.[13] This reaction responds to the addition of the effector molecules ATP, ADP and 2-OG in a manner very similar to that for PphA (compare Ref. 13) shown in Fig. 2b. P_{II}-P dephosphorylation is partially inhibited by ADP and ATP alone. The inhibition is strongly enhanced by the presence of 2-OG, whereas guanosine 5′-triphosphate (GTP) has no effect on P_{II}-P phosphorylation. Together, these assays revealed a high degree of functional similarity between Tll2243 and PphA, and therefore, we termed the tll2243 product tPphA.

Crystal structure of tPphA

Native crystals of tPphA were obtained under two different conditions in two different space groups: $C222_1$ with one monomer in the asymmetric unit and $P4_12_12$ with two monomers in the asymmetric unit. These orthorhombic crystals diffracted to a resolution of 1.28 Å. Crystals in $P4_12_12$ diffracted only after soaking with the substrate *p*-NPP for 1 h. The resolution obtained with these tetragonal crystals at a synchrotron was not better than 3.05 Å. Selenomethionine (Se-Met) crystals were obtained only in space group $C222_1$ (Table 1). The structure in the orthorhombic space group was initially determined using multiple wavelength dispersion (MAD). The structure in the tetragonal space group was solved by molecular replacement (MR) using the monomer from the orthorhombic space group as a search model (Table 2).

The overall fold of all three monomers of tPphA contains the common secondary elements of PP2C phosphatases:[20] a central beta sandwich consisting of two five-stranded, antiparallel beta sheets surrounded by two pairs of antiparallel alpha-helices (Fig. 3a–c). The three structures are very similar in their overall structure except for the flap region comprising amino acids 138 to 165 (Fig. 4a). This region is very flexible in the tPphA structure in $C222_1$ and could only be built from amino acids 138 to 143 and 160 to 165 (amino acids 142, 143, 160 and 161 only backbone). In both monomers in $P4_12_12$ the flap region is well ordered except for amino acids 146 to 150 in monomer A and amino acids 146 to 149 in monomer B. The high degree of flexibility of this part is clearly shown in the differences between the two monomers in the tetragonal space group: in monomer A the flap region is forming a loop region, whereas in monomer B this region is partially helical (amino acids 138 to 145 and 157 to 161). An inte-

Table 1. Data collection 2 and refinement statistics

	Native crystal in $C222_1$	Native crystal in $P4_12_12$
Data collection		
Wavelength (Å)	1.0500	0.97629
Space group	$C222_1$	$P4_12_12$
Cell parameters (Å)		
a	38.94	113.29
b	152.13	113.29
c	82.44	88.61
Resolution (Å)	1.28 (1.38–1.28)	3.05 (3.15–3.05)
Redundancy	0.99 (0.98)	1.86 (1.83)
Completeness (%)	99.2 (98.0)	99.9 (98.7)
Mean $I/\sigma(I)$	25.01 (3.32)	15.73 (5.22)
R_{int} (%)	6.44 (52.45)	3.72 (16.18)
Refinement		
R_{cryst}	16.33	24.02
R_{free}	20.42	29.50
Protein atoms	1822	3434
Heteroatoms	3	6
Water molecules	136	13
Mean *B* value (Å^2)	27.75	42.62
Main chain	25.59	42.59
Side chains	29.81	42.66
Standard uncertainties		
Bond length (Å)	0.013	0.007
Bond angle (deg)	0.036	1.303
Ramachandran plot (%)		
Most favoured region	92.4	81.1
Allowed region	7.6	18.7
Generally allowed region	0	0.2
Disallowed region	0	0

Table 2. Data collection 1

Data	Se peak	Se inflection	Se high remote
Wavelength (Å)	0.9792	0.9796	0.9500
Space group	$C222_1$	$C222_1$	$C222_1$
Cell parameters (Å)			
a		38.94	
b		152.13	
c		82.44	
Resolution (Å)	2.06 (2.16–2.06)	2.06 (2.16–2.06)	2.06 (2.16–2.06)
Redundancy	14.32 (13.98)	7.00 (5.90)	7.11(6.74)
Completeness (%)	99.5 (97.8)	97.7 (82.6)	99.5 (98.3)
Mean $I/\sigma(I)$	42.33 (20.37)	31.54 (14.22)	28.58 (12.01)
R_{int} (%)	4.94 (14.22)	4.12 (13.53)	4.02 (15.06)

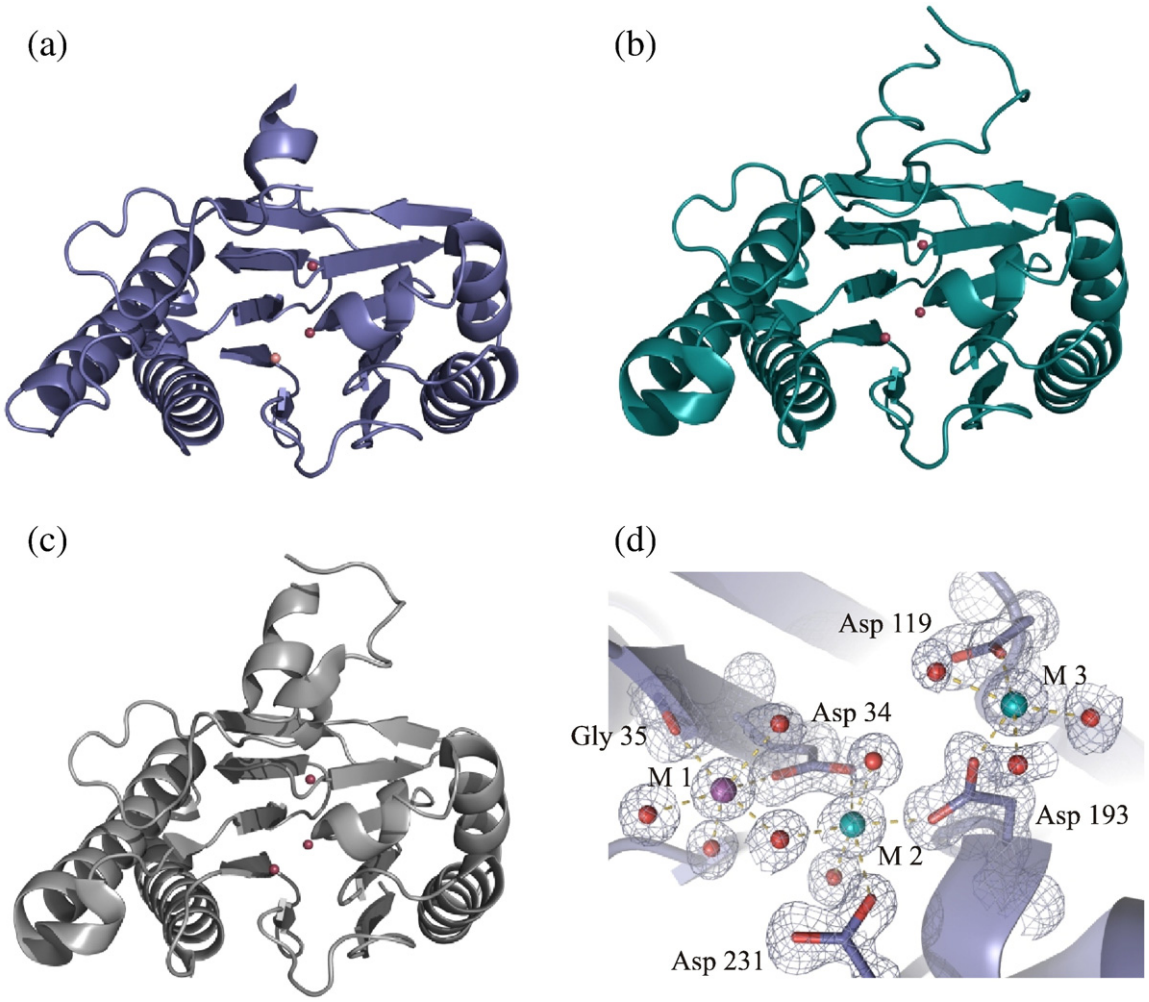

Fig. 3. Structure of tPphA in different space groups and the active site. (a) tPphA structure in $C222_1$. The metal ions are shown as spheres: Mg^{2+}, pink; Ca^{2+} and mixture of Mg^{2+} and Ca^{2+}, dark pink. All structural figures were generated with PyMOL [http://pymol.sourceforge.net]. (b) tPphA structure in $P4_12_12$ monomer A. (c) tPphA structure in $P4_12_12$ monomer B. (d) Active site of tPphA in $C222_1$. M1: Mg^{2+}, M2: mixture of Mg^2 and Ca^{2+}, M3: Ca^{2+}. Hydrogen bonds are shown with dashed lines.

resting difference between the $C222_1$ structure and $P4_12_12$ structure is the different orientation of Arg169 near the flap region (Fig. 4b). In $C222_1$, Arg169 is shifted towards the backbones of Asp95 and Met96 and is building hydrogen bonds to them (3.28 and 3.41 Å for the side chain of Arg169 and the backbone of Asp95, respectively, and 3.08 Å for the side chain of Arg169 and the backbone of Met96). In $P4_12_12$, Arg169 is turned towards the flap region. In monomer A the side chain of Arg169 is building a very weak hydrogen bond with the backbone of Leu163 (3.77 Å), whereas the side chain of Arg169 in monomer B is too far away from Leu163 to form a hydrogen bond. The different orientation of Arg169 could be involved in the structural rearrangements of the flap subdomain (see below).

Active site of tPphA

All three monomers of tPphA bind three metal ions in the active site similar to the PstP structure from *M. tuberculosis*,[16] the MspP structure from *M. smegmatis*[17] and the STP structure from *S. agalactiae*.[19] In the monomer in the orthorhombic space group there is one fully occupied magnesium ion from the purification procedure, one fully occupied calcium ion from the crystallization condition and one metal ion comprising a mixture of magnesium and calcium. In the tetragonal space group, the two monomers have three fully occupied magnesium ions from soaking of the crystal, but no *p*-NPP or phosphate molecule could be observed in the electron density.

The coordination sphere of the three metal ions is formed by Asp34, Gly35, Asp119, Asp193 and Asp231 in both space groups (Fig. 3d). In the tPphA structure in $C222_1$, nine water molecules complete the coordination of the metal ions. Metal ion M1 is coordinated by four water molecules, one main-chain oxygen of Gly35 and one side-chain oxygen (OD1) of Asp34. Metal ion M2 (mixture of Mg^{2+} and Ca^{2+}) is coordinated by three water molecules and one side-chain oxygen each of Asp34 (OD2), Asp193

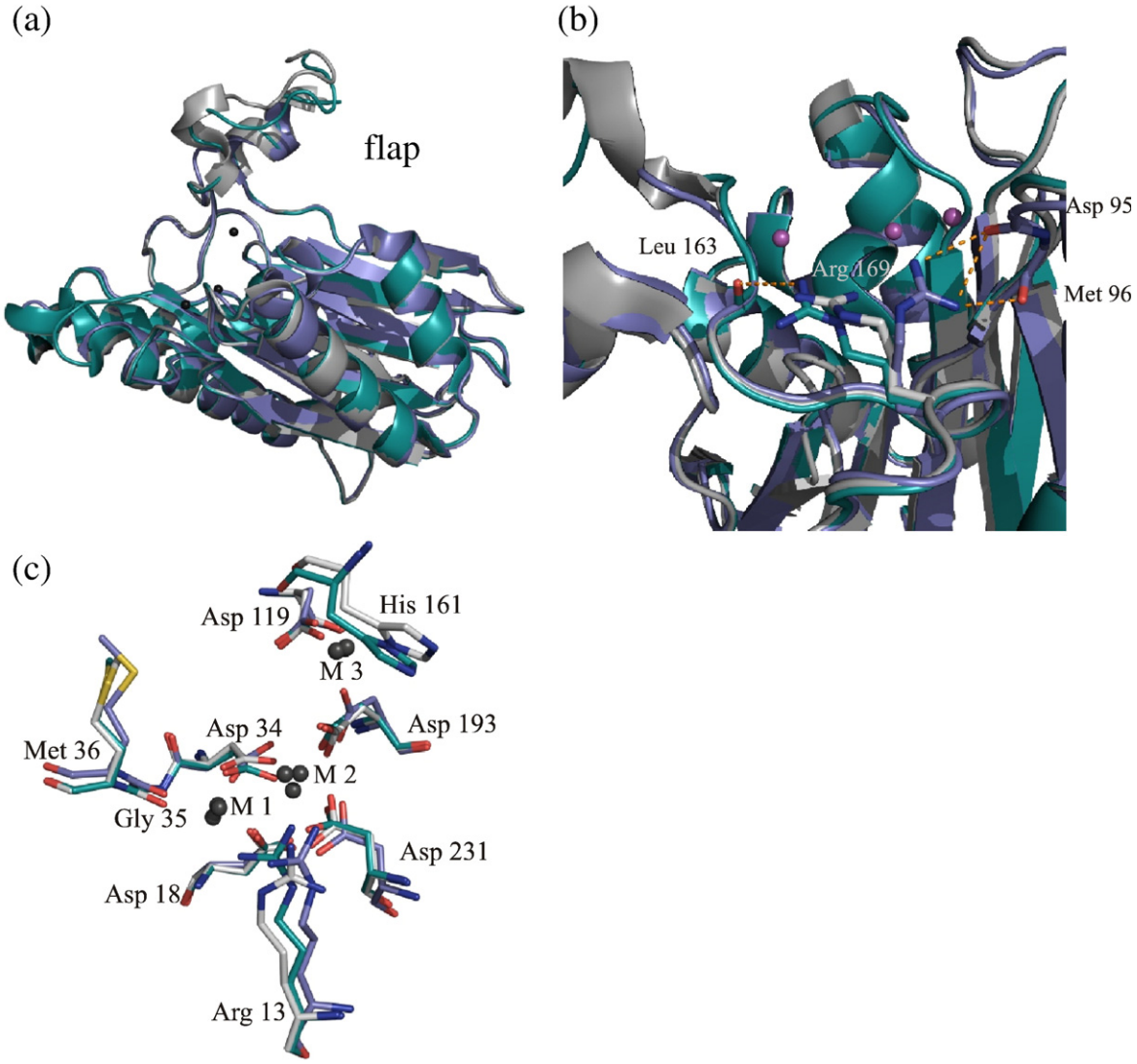

Fig. 4. Comparison of the different tPphA monomers. (a) Superposition of the three monomers of tPphA from different space groups. Blue: tPphA in $C222_1$, cyan: tPphA monomer A in $P4_12_12$, grey: tPphA monomer B in $P4_12_12$. (b) Different position of Arg169 in the three tPphA monomers. Hydrogen bonds are shown with dashed lines. (c) Superposition of the active site in the three tPphA monomers. Metal ions are shown in black. Blue, tPphA in $C222_1$; cyan, tPphA monomer A in $P4_12_12$; grey, tPphA monomer B in $P4_12_12$.

(OD1) and Asp231 (OD2). These two metal ions are octahedrally coordinated. The coordination sphere of the third metal M3 is formed by three water molcules and one side-chain oxygen each of Asp119 (OD2) and Asp193 (OD2); a sixth coordination site is free (Fig. 3d). In the tPphA structure in $P4_12_12$, the coordination spheres of the three metal ions are less complete because of missing water molecules that could not be built because of the modest resolution. However, the amino acids coordinating the metal ions are the same as in $C222_1$ (Fig. 4c). Also in $P4_12_12$, the sixth coordination site of the third metal ion is free.

Overall, the amino acids that coordinate the three metal ions have very similar positions in the three monomers of tPphA. Nevertheless, the catalytic centre in the three monomers exhibits slight differences with respect to the exact position of the metal ions and amino acids Arg13, Asp34, Asp193 and Asp231 (Fig. 4c). Arg13, which is responsible for substrate binding in the active site, has a slightly different position in all three monomers. This suggests that soaking with the substrate *p*-NPP could induce some movements of Arg13. The most important difference concerns the position of Asp193. In $C222_1$, Asp193 is coordinating M2 by one side-chain oxygen (OD1) and M3 by the second side-chain oxygen (OD2). In the two monomers in $P4_12_12$, the Asp193 is shifted towards M2, which results in a longer distance between OD2 of Asp193 and M3 (monomer A, 3.33 Å; monomer B, 3.25 Å).

Comparison of the tPphA structures with other PP2C-like phosphatases

The overall ternary structure of tPphA corresponds to the structure of the catalytic domain of

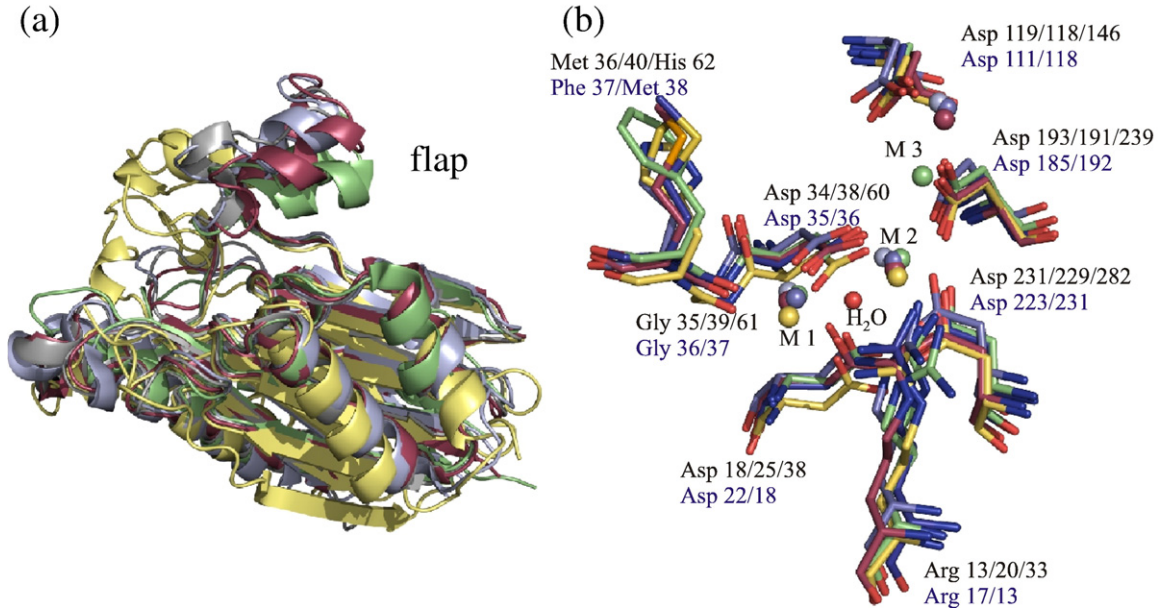

Fig. 5. Comparison of PP2C, PstP, MspP, STP and tPphA. (a) Superposition of PP2C, PstP, MspP, STP and tPphA: yellow, PP2C; red, PstP; green, MspP; light blue, STP monomer C; grey, tPphA monomer B ($P4_12_12$). For clarity, the PP2C structure is shown without the three alpha-helices at the C-terminus. (b) Superposition of the active sites of PP2C (yellow), PstP (red), MspP (green), STP (light blue) and tPphA in $C222_1$ (dark blue). The denotation of the amino acids is as follows: first line, first position tPphA, second position PstP and third position PP2C (black); second line, first position MspP, second position STP (purple).

human PP2C and of bacterial PstP, MspP and STP (Fig. 5a) except that the bacterial PP2C members lack three alpha-helices at the C-terminus that are present in human PP2C. The active sites of all five PP2C-like structures (human PP2C, tPphA, MspP, STP and PstP) are highly conserved, all containing the characteristic amino acids, which are required for Me^{2+} coordination (Fig. 5b).

A main difference between human PP2C and the four bacterial phosphatases is the number of metal ions. In the human PP2C, only two metal ions in the active centre have been described, whereas in the bacterial enzymes tPphA, STP, PstP and MspP, three metal ions are present. The two metal ions in the catalytic centre of the human PP2C are at positions identical to that of the metal ions M1 and M2 in the bacterial homologues. In addition, the latter structures contain a third metal ion, which was not visible in human PP2C. Because of different crystallization buffers, the third metal is a magnesium ion in the case of tPphA and STP, whereas in PstP and MspP (Protein Data Bank entry 2jfs), the metals are manganese ions. The third metal ion M3 is coordinated differently in the structures of the four bacterial phosphatases: In the case of PstP the metal ion M3 (Mn^{2+}) is coordinated by three amino acids: Asp118, Asp191 and Ser160 (Fig. 6) with hydrogen bond distances of 1.89, 2.27, and 2.15 Å/2.06 Å, respectively. In the high-resolution MspP structure (2jfs), there are three hydrogen bonds to M3: one from Asp185 (2.09 Å) and one from His153 (2.22 Å) and a third coordination to M3 built by the phosphate molecule (2.09 Å).

In the structures of tPphA and STP, only two amino acids are located near the third metal ion: in the tPphA structure they are Asp119 (equivalent to

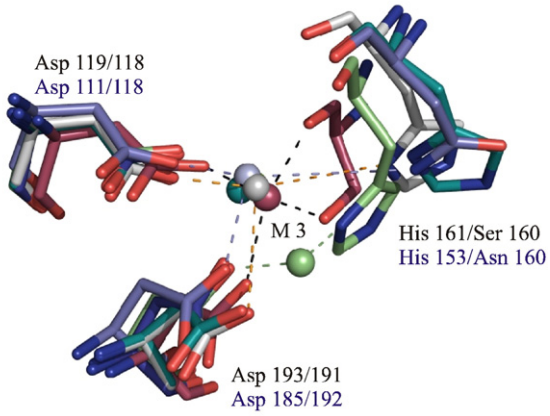

Fig. 6. Comparison of the coordination sphere of the third metal ion in PstP, MspP, STP and tPphA. Red, PstP; light blue, STP; dark blue, tPphA in $C222_1$ (His161 is not visible in the electron density); cyan, tPphA monomer A in $P4_12_12$; grey, tPphA monomer B in $P4_12_12$; green, MspP. Hydrogen bonds (dashed lines) concerning the PstP structure are shown in black, hydrogen bonds concerning the tPphA structure are shown in orange, hydrogen bonds concerning the MspP structure are shown in green and hydrogen bonds concerning the STP structure are shown in light blue. The denotation of the amino acids is as follows: first line, first position tPphA, second position PstP (black); second line, first position MspP, second position STP (purple).

Asp118 in PstP and STP) and Asp193 (corresponding to Asp191 in PstP and Asp192 in STP). The third coordinating residue in PstP, Ser160, is missing in tPphA and STP. A third amino acid for the coordination of M3 coming from the flap region could be His161 in the case of tPphA (located at the position corresponding to PstP Ser160) and Asn160 in the case of STP, but in all monomers the NH group is too far away from the third metal ion (tPphA: monomer A, 4.38 Å; monomer B, 3.88 Å; STP: monomer C, 4.34 Å). Interestingly, the His161 in tPphA and the His153 in MspP are located very near to each other.

Furthermore, only in the tPphA structure in $C222_1$, residues Asp118 and Asp193 bind to M3 (distances: 1.92 and 2.27 Å, respectively), whereas in $P4_12_12$, Asp193 is too far away from the third metal ion.

Another remarkable difference between human PP2C and its bacterial counterparts concerns His62 of human PP2C, which was shown to function as an acid in the splitting of the P–O bond.[20] In the case of tPphA, MspP, STP and PstP, the homologous position is occupied by a methionine residue (Met36 in tPphA, Met38 in STP and Met40 in PstP), whereas in the case of MspP this position is occupied by a phenylalanine (Phe37), shown in Fig. 5b.

The region with the most striking structural differences between tPphA and the four hitherto described PPM structures corresponds to the flap subdomain comprising amino acids 153 to 161 in the tPphA structures. This region is much more flexible in the tPphA structures than in the others (see above). Most remarkably, a structural rearrangement of the tPphA flap region was observed upon addition of the substrate *p*-NPP. A superposition of the five phosphatases (Fig. 5a) shows that the flap region in the PP2C structure is shifted away from the active site; in the PstP and MspP structure it is located nearer to the active site, and in the tPphA and STP structures this region is nearest to the active site.

Mutational analysis of tPphA

To further examine the significance of residues in the flap subdomain of tPphA with respect to its enzymatic activity, four tPphA mutants were generated by site-directed mutagenesis. Residue His161, located in the vicinity of the catalytic cleft and occupying the position of the M3-liganding Ser160 of *M. tuberculosis* PstP, was replaced by either serine or alanine (termed H161S and H161A, respectively). Another noticeable residue, Trp159, projects from the base of the flap and seems to shield the active site (molecule B in $P4_12_12$). This residue was replaced by alanine (W159A). Finally, Arg 169, whose side chain exhibits a marked movement in the different space groups of tPphA (see above), was replaced by alanine (R169A). When assayed with *p*-NPP as artificial substrate, only the Arg169 mutation caused a pronounced impairment of activity. Both K_M and V_{max} were negatively affected, and consequently, the overall catalytic efficiency was only one-third of that of the wild-type enzyme. By contrast, mutation of Trp159 or His161 only slightly affected activity (Table 3). In the mutants W159A and H161S, both the K_M and V_{max} increased, resulting in an overall catalytic efficiency that is similar to that of the wild-type protein. Compared to H161S, H161A showed a modestly higher increase in K_M and a lower increase in V_{max}. The consequence of the tPphA mutations on thermostability, and thus, on structural integrity, was examined by preincubating the enzymes for 15 min at different temperatures, followed by assaying the activities with *p*-NPP as substrate. Preincubations were carried out under both reducing and nonreducing conditions. As shown in Fig. 7, there is a tremendous overall effect of the reducing conditions on thermostability. In the absence of DTT, the enzymes lose activity much more rapidly than in the presence of 5 mM DTT. Of the various mutations, the R169A mutation showed the most pronounced loss of thermostability, in particular under nonreducing conditions. The reactivity of the various mutants towards the natural substrate, P_{II}-P, was tested in the absence of inhibitory effector molecules. Similar to that observed for *p*-NPP reactivity, the R169A mutation caused a marked impairment of P_{II}-P dephosphorylation activity, whereas only a slight impairment of activity was observed in H161S, H161A and W159A mutants (Fig. 8). Inhibition of P_{II}-P dephosphorylation by the effector molecules ATP and 2-OG was not affected by the tPphA mutations (not shown), which is expected, since the effectors bind to the P_{II} protein and do not directly affect the phosphatase[13] (see below). It seems that Arg169 is more important for both the activity and the stability of tPphA than flap residues Trp159 and His161, in agreement with the proposed role of Arg169 as hinge of the flap subdomain, illustrated by the large side-chain movement between the different space groups of the tPphA crystals.

Table 3. Kinetic constants of tPphA and derived mutants for *p*-NPP hydrolysis activity

tPphA enzyme	K_M (mM)	V_{max} (U/mg)	K_{cat}/K_M
WT	0.75	20	26.6
H161S	1.4	37	26.4
H161A	1.7	30	17.6
W159A	1.2	30	25.0
R167A	1.5	16	10.6

p-NPP hydrolysis assays were carried out as described in Materials and Methods. To determine the kinetic constants, assays were performed in the presence of 0.125, 0.25, 0.5, 0.75, 1.5, 2.0 and 2.5 mM *p*-NPP. From the apparent reaction velocities, the kinetic constants were calculated by hyperbolic fitting using the GraphPad prism 4.0 program. Triplicate assays were used with standard deviations of less than 5%.

Conclusions

This study revealed the structure of the PphA homologue from *T. elongatus*, a small soluble protein phosphatase of the PPM family, which consists only of the catalytic domain, lacking C- or N-terminal substrate binding or regulatory domains. Never-

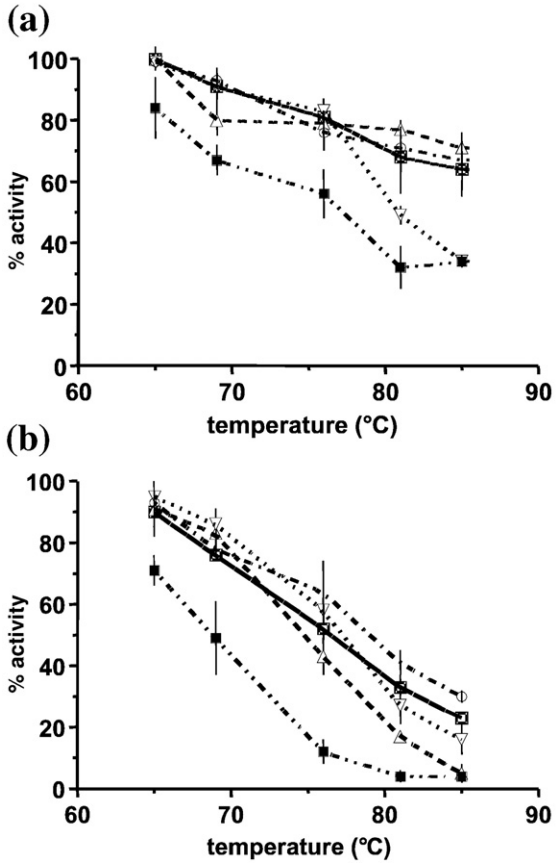

Fig. 7. Thermostability of wild-type tPphA protein and four mutant variants [wild-type tPphA (□), mutant W159A (▲), H161A (▼), H161S (♦) and R169A (●)]. The purified tPphA proteins were diluted in a buffer (20 mM Hepes, pH 7.4, 50 mM KCl, 5 mM $MgCl_2$, 0.5 mM EDTA) with 5 mM DTT (a) or without DTT (b) and incubated at different temperatures as indicated for 15 min. Thereafter, the activity of the proteins was assayed for *p*-NPP hydrolysis activity under standard assay conditions as described in Materials and Methods. The 100% activity refers to the activity of the enzyme that was not heat-treated.

theless, PphA recognizes its substrate in a highly specific manner, since in a PphA-deficient mutant, dephosphorylation of the signalling protein P_{II}-P is strongly impaired in spite of the presence and activity of other PPM homologues.[15] The present structure shows that despite a low sequence conservation, the overall structure of the PPM core is highly conserved. Almost all universally conserved amino acids are involved in binding of the metal ions in the active centre. Accordingly, the metal centre consisting of M1 and M2, including the catalytically active bridging water, is almost identical in all known PPM structures. The binding of the third metal in PstP, which was not reported in human PP2C, was attributed to a particular structure of the flap subdomain providing a ligand for M3, Ser160. However, in the present tPphA structure, no coordination of M3 was observed from residues of the flap. Residue Ser160 is not conserved in tPphA and the structure of the flap subdomain is different; nevertheless, M3 is located at an almost identical position compared to PstP. Therefore, it seems that coordination of M3 from the flap subdomain is not necessary for binding. This conclusion is also supported by site-directed mutagenesis of the residue (His161) corresponding to either alanine or serine, which resulted in no substantial loss of enzymatic activity or structural integrity, as concluded from the thermostability of these mutants.

According to the new structural data presented here, the conserved residues Asp119 and Asp193 of tPphA seem to be sufficient to bind M3. However, these residues are also present in human PP2C. This raises the question of whether human PP2C may also contain a third metal at this place. Since the crystallization of this enzyme was carried out in a buffer at pH 5 where the enzyme shows little activity,[24] the third metal may have been lost under the particular crystallization conditions. When MspP was crystallized in a buffer of pH 5.5, the third metal was indeed lost.[18] Considering the universal conservation in all PPM members of those aspartate residues, which coordinate the third metal in MspP, PstP, STP and tPphA, the trinuclear metal centre may be a general feature of protein phosphatases of the PPM family.

A second major novel insight into the structure–function relationship of PPM enzymes concerns the function of the flap subdomain. The present structure revealed that this subdomain is highly flexible. Only after soaking the crystal with magnesium ions and the artificial substrate *p*-NPP could an ordered structure be obtained in space group $P4_12_12$. Significantly, the major difference between the two monomers concerns the structure of the flap subdomain. In one of those (molecule B), the activated water molecule is not visible and the flap seems to be more open with respect to the catalytic cleft than in

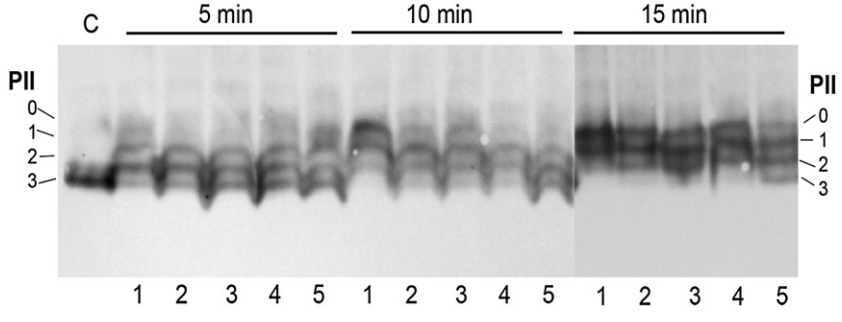

Fig. 8. Time course of P_{II}-P dephosphorylation by wild-type tPphA (1) and mutant proteins W159A (2), H161A (3), H161S (4) and R169A (5). Reactions were started as described under Materials and Methods and were stopped after 5, 10 and 15 min on ice followed by determination of P_{II} phopshorylation state by nondenaturing PAGE and immunoblot analysis.

molecule A. Thus, molecule B could represent the enzymatic state after substrate hydrolysis and release are performed. Mutational analysis of the flap subdomain showed that mutation of Arg 169 caused the most pronounced effect on enzymatic activity. This amino acid seems to take part in the structural organisation of the flap domain, since the arginine side chain makes a 90° side-chain movement between the $C222_1$ and $P4_12_12$ structures. On the other hand, mutation of His161 or Trp159, which are located in the vicinity of the catalytic cleft, seems to have only a minor impact on the catalytic efficiency of the enzyme. Mutation of residue Ser160 in PstP (corresponding to tPphA His161) to Ala had a similar modest effect on *p*-NPP hydrolysis activity.

In this respect, it is interesting to note that these mutations increased the K_M for the substrate *p*-NPP and concomitantly also increased V_{max} (except for R169A). This indicates that the flap domain is involved in substrate binding and turnover. A more open flap (exchange of the bulky tyrosyl or histidyl side chains at the entrance of the catalytic cleft by smaller alanyl/seryl side chains) may at the same time facilitate substrate exchange (positively affecting V_{max}) and decrease its affinity for binding the catalytic site. Dephosphorylation of the physiological substrate P_{II}-P was also affected by mutation in the flap subdomain. In contrast to *p*-NPP hydrolysis, where the overall catalytic activity was not affected by Tyr159 and His161 mutation, dephosphorylation of P_{II}-P was negatively affected, although modestly. Since the turnover with the substrate P_{II}-P by tPphA and by PphA (also shown previously by Ruppert *et al.*[13]) is much slower than the hydrolysis of *p*-NPP, binding of the phosphorylated seryl residue of the T loop to the catalytic cleft may be the rate-limiting step in P_{II}-P dephosphorylation. The flexibility of the flap domain and interactions of flap domain residues with T-loop residues may be involved in the specificity of this process. Binding of effector molecules to P_{II} proteins was recently shown to dramatically affect the structure of the T-loop conformation.[25] The narrow catalytic cleft shielded by a flexible flap subdomain may provide the structural prerequisite that allows dephosphorylation of phosphoseryl residue 49 of P_{II} only when the T loop adopts a conformation with no 2-OG bound. Binding of ATP and ADP would cause T-loop structures in which the access of the phosphoseryl residue is more difficult, leading to partial inhibition of dephosphorylation by wild-type tPphA as well as by the three tPphA mutants. It remains to be elucidated to which extent the flap domain is involved in the specificity of substrate selection.

Materials and Methods

Cloning, overexpression and purification of untagged native enzyme tPphA

tPphA, encoded from *Thermosynechococcus*, was cloned into the pET32a-Vector (Novagen) by using the following primer combination: 5′-GGA ATT CCA TAT GGA CGT TGC TGG CTT AAC-3′ with an NdeI site and 5′-CCG CTC GAG CGG TTA AAC ACT GAT GAC AAC GAC G-3′ with an XhoI site. The construct was transformed into *E. coli* BL21 (DE3) cells and expression was carried out in LB medium at 15 °C overnight after induction with 1 mM IPTG at $OD_{600} = 0.6$. After 20 h induction, the cells were harvested through centrifugation and lysed by sonification on ice in buffer 1 [20 mM Hepes, pH 7.4, 50 mM KCl, 5 mM $MgCl_2$, 0.5 mM ethylenediaminetetraacetic acid (EDTA), 0.2 mM PMSF, 3 mM DTT] supplemented with COMPLETE™ (Roche). The purification was done at 4 °C. The lysate was centrifuged for 1 h at 38,000 rpm. Ammonium sulfate was added to the following saturations: 35%, 50%, 60% and 65%. After every step, the precipitate was collected by centrifugation and resuspended in 2 ml buffer 1. The fractions containing tPphA were dialyzed against 2 l of buffer 1 and applied to a HiTrap Q XL (Amersham Pharmacia) anion exchange column, which was equilibrated in buffer 1. tPphA was eluted at a flow rate of 1 ml/min by a 40-ml linear gradient from 50 to 600 mM KCl. Protein fractions were pooled and concentrated to 2 ml on a Vivaspin Centriprep with 10,000 MWCO before gel filtration on a Superdex 75 16/60 column (GE Lifesciences). The column was equilibrated with buffer 2 (150 mM NaCl, 20 mM Hepes, pH 7.4, 50 mM KCl, 5 mM $MgCl_2$, 0.5 mM EDTA and 3 mM DTT). tPphA-containing fractions were pooled and concentrated to 52 mg/ml.

Overexpression and purification of untagged Se-Met enzyme tPphA

The expression construct of tPphA was transformed into the methionine auxotroph strain *E. coli* B834 (DE3). Se-Met-labelled protein was expressed in minimal media supplemented with Se-Met according to the EMBL protein expression group† and purified according to the protocol described above. The selenolabelled protein was purified in the same way as the native protein and the final concentration was adjusted to 58 mg/ml.

Crystallization

Initial crystallization trials for the native protein were carried out with a Mosquito robot (TTP Labtech) by using the Wizard screen I and II (Emerald) and the Index screen (Hampton Research). All crystallization experiments were performed at 20 °C with a protein concentration of 36 mg/ml. Crystallization conditions were refined by using hanging drops containing a 0.8 µl:0.8 µl mixture of protein and reservoir solution. Conditions for native and Se-Met protein in space group $C222_1$ are 0.2 M $CaCl_2$, 0.1 M Tris, pH 7.0 and 23% PEG 3350. Crystallization conditions for native crystals in space group $P4_12_12$ are 0.2 M $CaCl_2$, 0.1 M Hepes, pH 8.0 and 28% PEG 3350. For X-ray data collection, crystals were soaked in a solution containing the reservoir solution and 15% 2,3-butanediol as cryoprotectant. The crystals were also tested for their catalytic activity by transferring them into a solution containing in the first case 0.2 M $CaCl_2$ and 25 mM *p*-NPP additional to the reservoir solution, in the second case 0.2 M $MnCl_2$ and 25 mM *p*-NPP and in the third case 0.2 M $MgCl_2$ and 25 mM *p*-NPP. After 1 h, the yellow colour of *p*-NPP was visible in the solutions containing $MnCl_2$ and $MgCl_2$. The

† http://www.embl-heidelberg.de

native crystals in space group $P4_12_12$ did not diffract until they were soaked in solution containing *p*-NPP and 0.2 M $MgCl_2$.

Data collection and processing

Data sets with native and Se-Met crystals in space group $C222_1$ were collected at DESY in Hamburg at BW 6. The native crystal data sets—high and low resolution—were collected at 1.0500 Å. For the Se-MAD experiment, a fluorescence scan was done to determine the peak and inflection wavelength. The Se-MAD data sets were collected as follows: peak data set first, inflection data set second and high remote data set last on one single Se-Met crystal. The native crystal data set in space group $P4_12_12$ was collected at the SLS at PX 6. Data collection statistics are shown in Tables 1 and 2. All data were processed with HKL2000.[26]

Structure determination and refinement

The structure in $C222_1$ was solved by using SHELXC/D/E.[27,28] Three Se-Met sites could be identified. The initial model was built using ARP/wARP,[29] resulting in modeling of 79.6% of the structure and was refined using REFMAC5.[30] After completing the model by manual model building with COOT[31] followed by positional and *B*-factor refinement with REFMAC5[30] coupled with ARP solvent building, the refinement for modelling disorder and occupancies was switched to SHELXL.[32] The final model contains one monomer of tPphA (residues 37 to 40 and 144 to 159 were disordered), three cations (mixture of Ca^{2+}/Mg^{2+}) and 136 water molecules in the asymmetric unit.

The structure in $P4_12_12$ was solved by molecular replacement using PHASER.[33] First a rigid-body refinement followed by simulated annealing and bgroup refinement was done with CNS.[34] Manual model building was done with COOT[31] followed by simulated annealing and individual *B*-factor refinement in CNS.[34] After the model was completed, water molecules were picked with CNS.[34] The final model consists of two monomers of tPphA (residues 146 to 150 were disordered), six magnesium ions and, because of the modest resolution, only 13 water molecules in the asymmetric unit. Statistics of the Ramachandran plot and the refinement statistics are shown in Table 2.

Construction of tPphA mutants

Plasmid pET-32a(+) carrying the tPphA gene from *T. elongatus* strain BP-1 (see above) was mutated by site-directed mutagenesis with oligonucleotides employing the megaprimer PCR method as described by Sambrook and Russell.[35] For the synthesis of the megaprimers, the following oligonucleotides were used: the primer TlrRev (5′-GCCCGCCGTGGGTTTTGGC-3′) was used as universal reverse primer; for construction of the W159A mutation, the primer TlrW-AFw (5′-GCATCCGGCGCGCCATGTGC-3′) was used; for H161S, TlrH-SFw (5′-ATCCGTGGCGCAGTGTGCTCT-3′), for H161A, TlrH-AFw (5′-ATCCGTGGCGCGCTGTGCTCT-3′) and for R169A, TlR-Afw (5′-GTGTTTAGGAGCCGAGGACCTC-3′). The PCR products containing the mutations were separated from wild-type template plasmid by restriction with DpnI, which cleaves fully methylated $G^{Me6}ATC$ sequences. All constructs were checked by sequencing.

Assay of Tlr2243 phosphatase activity

Phosphatase activity with *p*-NPP as substrate was assayed as described by Mackintosh[36] for wild-type tPphA and H159S, H159A, W157A and R167A mutant enzymes. The standard 1-ml assays were carried out in buffer consisting of 20 mM Tris–Cl, pH 8.3, 50 mM NaCl, 2 mM $MnCl_2$ and 1 mM DTT at room temperature with *p*-NPP substrate concentrations between 0.125 and 2.5 mM. Reactions were started by the addition of purified enzyme (0.34 μg). The increase in absorbance at 400 nm was recorded on an Ultrospec 3000 spectrophotometer (Amersham-Pharmacia) against a blank reaction without enzyme. The linear slope of the reaction plot was used to determine the reaction velocity at a given substrate concentration. From these values, the kinetic constants K_m and V_{max} were calculated by nonlinear hyperbolic fitting using the program GraphPadPrism 4.0 (GraphPad Software, San Diego, CA).

In vitro Tlr2243 phosphatase reactivity towards P_{II}-P

The P_{II}-P-specific phosphatase activity was tested for wild-type tPphA and the H159S, H159A, W157A and R157A mutant enzymes. Ten-microliter reactions were carried out in a buffer containing 10 mM Tris–Cl, pH 7.4, 10 mM $MgCl_2$, 50 mM NaCl, 1 mM DTT, 5 mM benzamidine, 10 μg bovine serum albumin, 0.05% NP40, 10% Xylitol and 20 ng purified P_{II}-P together with effector molecules, when indicated. The reactions were started by the addition of 30 ng of purified enzyme. After incubation at 37 °C for the indicated time intervals, the reactions were stopped on ice. Subsequently, the phosphorylation state of P_{II} was determined by nondenaturing PAGE and immunoblot analysis as described previously.[37]

Protein Data Bank accession numbers

The coordinates and structure factors of the two tPphA structures have been deposited in the Protein Data Bank with the entry codes 2j82 and 2j86.

Acknowledgements

We thank Carmen Haas for expert technical assistance and gratefully acknowledge financial support from the DFG (grant Fo195/4). Furthermore we thank Gleb Bourenkov and Ehmke Pohl for assistance with data collection.

References

1. Kennelly, P. J. (2002). Protein kinases and protein phosphatases in prokaryotes: a genomic perspective. *FEMS Microbiol. Lett.* **206**, 1–8.
2. Shi, L. (2004). Manganese-dependent protein *O*-phosphatases in prokaryotes and their biological functions. *Front. Biosci.* **9**, 1382–1397.
3. Zhang, C. C., Jang, J., Sakr, S. & Wang, L. (2005). Protein phosphorylation on Ser, Thr and Tyr residues in cyanobacteria. *J. Mol. Microbiol. Biotechnol.* **9**, 154–166.

4. Zhang, W. & Shi, L. (2004). Evolution of the PPM-family protein phosphatases in *Streptomyces*: duplication of catalytic domain and lateral recruitment of additional sensory domains. *Microbiology*, **150**, 4189–4197.
5. Treuner-Lange, A., Ward, M. J. & Zusman, D. R. (2001). Pph1 from *Myxococcus xanthus* is a protein phosphatase involved in vegetative growth and development. *Mol. Microbiol.* **40**, 126–140.
6. Wang, L., Sun, Y. P., Chen, W. L., Li, J. H. & Zhang, C. C. (2002). Genomic analysis of protein kinases, protein phosphatases and two-component regulatory systems of the cyanobacterium *Anabaena* sp. strain PCC 7120. *FEMS Microbiol. Lett.* **217**, 155–165.
7. Forchhammer, K. (2004). Global carbon/nitrogen control by PII signal transduction in cyanobacteria: from signals to targets. *FEMS Microbiol. Rev.* **28**, 319–333.
8. Forchhammer, K., Irmler, A., Kloft, N. & Ruppert, U. (2004). P signalling in unicellular cyanobacteria: analysis of redox-signals and energy charge. *Physiol. Plant*, **120**, 51–56.
9. Arcondeguy, T., Jack, R. & Merrick, M. (2001). PII signal transduction proteins, pivotal players in microbial nitrogen control. *Microbiol. Mol. Biol. Rev.* **65**, 80–105.
10. Forchhammer, K. (2007). PII Signal Transducers: Novel functional and structural insights. *Trends Microbiol.*, in press.
11. Ninfa, A. J. & Jiang, P. (2005). PII signal transduction proteins: sensors of alpha-ketoglutarate that regulate nitrogen metabolism. *Curr. Opin. Microbiol.* **8**, 168–173.
12. Kloft, N. & Forchhammer, K. (2005). Signal transduction protein PII phosphatase PphA is required for light-dependent control of nitrate utilization in *Synechocystis* sp. strain PCC 6803. *J. Bacteriol.* **187**, 6683–6690.
13. Ruppert, U., Irmler, A., Kloft, N. & Forchhammer, K. (2002). The novel protein phosphatase PphA from *Synechocystis* PCC 6803 controls dephosphorylation of the signalling protein PII. *Mol. Microbiol.* **44**, 855–864.
14. Irmler, A. & Forchhammer, K. (2001). A PP2C-type phosphatase dephosphorylates the PII signaling protein in the cyanobacterium *Synechocystis* PCC 6803. *Proc. Natl Acad. Sci. USA*, **98**, 12978–129783.
15. Kloft, N., Rasch, G. & Forchhammer, K. (2005). Protein phosphatase PphA from *Synechocystis* sp. PCC 6803: the physiological framework of P_{II}-P dephosphorylation. *Microbiology*, **151**, 1275–1283.
16. Pullen, K. E., Ng, H. L., Sung, P. Y., Good, M. C., Smith, S. M. & Alber, T. (2004). An alternate conformation and a third metal in PstP/Ppp, the *M. tuberculosis* PP2C-family Ser/Thr protein phosphatase. *Structure*, **12**, 1947–1954.
17. Bellinzoni, M., Wehenkel, A., Shepard, W. & Alzari, P. M. (2007). Insights into the catalytic mechanism of PPM Ser/Thr phosphatases from the atomic resolution structures of a mycobacterial enzyme. *Structure*, **15**, 863–872.
18. Wehenkel, A., Bellinzoni, M., Schaeffer, F., Villarino, A. & Alzari, P. M. (2007). Structural and binding studies of the three-metal center in two mycobacterial PPM Ser/Thr protein phosphatases. *J. Mol. Biol.* **374**, 890–898.
19. Rantanen, M. K., Lehtio, L., Rajagopal, L., Rubens, C. E. & Goldman, A. (2007). Structure of *Streptococcus agalactiae* serine/threonine phosphatase. The subdomain conformation is coupled to the binding of a third metal ion. *FEBS J.* **274**, 3128–3137.
20. Das, A. K., Helps, N. R., Cohen, P. T. & Barford, D. (1996). Crystal structure of the protein serine/threonine phosphatase 2C at 2.0 A resolution. *EMBO J.* **15**, 6798–6809.
21. Chenna, R., Sugawara, H., Koike, T., Lopez, R., Gibson, T. J., Higgins, D. G. & Thompson, J. D. (2003). Multiple sequence alignment with the Clustal series of programs. *Nucleic Acids Res.* **31**, 3497–3500.
22. Bork, P., Brown, N. P., Hegyi, H. & Schultz, J. (1996). The protein phosphatase 2C (PP2C) superfamily: detection of bacterial homologues. *Protein Sci.* **5**, 1421–1425.
23. Laurent, S., Forchhammer, K., Gonzalez, L., Heulin, T., Zhang, C. C. & Bedu, S. (2004). Cell-type specific modification of PII is involved in the regulation of nitrogen metabolism in the cyanobacterium *Anabaena* PCC 7120. *FEBS Lett.* **576**, 261–265.
24. Fjeld, C. C. & Denu, J. M. (1999). Kinetic analysis of human serine/threonine protein phosphatase 2Calpha. *J. Biol. Chem.* **274**, 20336–20343.
25. Yildiz, O., Kalthoff, C., Raunser, S. & Kuhlbrandt, W. (2007). Structure of GlnK1 with bound effectors indicates regulatory mechanism for ammonia uptake. *EMBO J.* **26**, 589–599.
26. Otwinowski, Z. M. & Minor, W. (1997). Processing of X-ray diffraction data collected in oscillation mode. *Methods Enzymol.* **276**, 307–326.
27. Schneider, T. R. & Sheldrick, G. M. (2002). Substructure solution with SHELXD. *Acta Crystallogr., Sect. D: Biol. Crystallogr.* **58**, 1772–1779.
28. Sheldrick, G. M. (2002). Macromolecular phasing with SHELXE. *Z. Kristallogr.* **217**.
29. Lamzin, V. S. & Wilson, K. S. (1993). Automated refinement of protein models. *Acta Crystallogr., Sect. D: Biol. Crystallogr.* **49**, 129–147.
30. Murshudov, G. N., Vagin, A. A. & Dodson, E. J. (1997). Refinement of macromolecular structures by the maximum-likelihood method. *Acta Crystallogr., Sect. D: Biol. Crystallogr.* **53**, 240–255.
31. Emsley, P. & Cowtan, K. (2004). Coot: model-building tools for molecular graphics. *Acta Crystallogr., Sect. D: Biol. Crystallogr.* **60**, 2126–2132.
32. Sheldrick, G. M. & Schneider, T. R. (1997). SHELXL: high-resolution refinement. *Methods Enzymol.* **277**, 319–343.
33. McCoy, A. J., Grosse-Kunstleve, R. W., Storoni, L. C. & Read, R. J. (2005). Likelihood-enhanced fast translation functions. *Acta Crystallogr., Sect. D: Biol. Crystallogr.* **61**, 458–464.
34. Brunger, A. T., Adams, P. D., Clore, G. M., DeLano, W. L., Gros, P., Grosse-Kunstleve, R. W. *et al.* (1998). Crystallography & NMR system: a new software suite for macromolecular structure determination. *Acta Crystallogr., Sect. D: Biol. Crystallogr.* **54**, 905–921.
35. Sambrook, J. & Russell, D. W. (2001). *Molecular Cloning. A Laboratory Manual*, 3rd edit. Cold Spring Harbor Laboratory Press, Cold Spring Harbor, NY.
36. Mackintosh, C. (1993). Assay and purification of (serine/threonine) phosphatases. In *Protein Phosphorylation. A Practical Approach* (Hardie, D. G., ed), pp. 197–230, Oxford University Press, Oxford.
37. Forchhammer, K. & Tandeau de Marsac, N. (1994). The PII protein in the cyanobacterium *Synechococcus* sp. strain PCC 7942 is modified by serine phosphorylation and signals the cellular N-status. *J. Bacteriol.* **176**, 84–91.